

Plunging Airfoil Load Characteristics Equipped with Gurney Flap

F. Ajalli¹ and M. Mani^{2*}

1. Department of Mechanical and Aerospace Engineering, Science and Research Branch, Islamic Azad University

2. Department of Aerospace Engineering and Center of Excellence in Computational Aerospace Engineering, Amirkabir University of Technology

*Postal Code: 15875-4413, Tehran, IRAN

mani@aut.ac.ir

Numerous experiments have been conducted on plunging Eppler 361 airfoil in a subsonic wind tunnel. The experimental tests involved measuring the surface pressure distribution over the airfoil at $Re=1.5 \times 10^5$. The airfoil was equipped with Gurney flap (heights of 2.6, 3.3 and 5% chord) and plunged at 6cm amplitude. The unsteady aerodynamic loads were calculated from the surface pressure measurements, 51 ports, along with the chord on both upper and lower surfaces of the model. The Gurney flap effects over the loads hysteresis loops of the oscillating airfoil were particularly studied prior to stall, at the stall onset, in light stall, and deep stall conditions. The static results of the flapped and unflapped airfoil were also explored in order to make a reference of comparison to the dynamic loads. The results showed that, the addition of the Gurney flap provided no changes in the directions of the C_l , C_d and C_m hysteresis loops for the prior to stall flow conditions; while as a result of the positive camber effects, the lift hysteresis loops shifted upward and the pitching moment's loops moved vertically downward. Additionally, adding the Gurney flap promoted dynamic stall phenomena. The deep dynamic stall of the flapped airfoil with the height of $h/c=5\%$ was seen at $\alpha_{ds}=13.1deg$. This phenomenon was observed at $\alpha_{ds}=14.8deg$ for the flapped airfoils of $h/c=2.6$ and 3.3% .

Keywords: Plunging airfoil, Gurney flap, Aerodynamic loads, Dynamic stall

Nomenclature

c	Airfoil chord
C_l	Lift force coefficient
C_d	Drag force coefficient
C_m	Pitching moment coefficient
H	Instantaneous displacement of the plunging motion (cm)
h_0	Amplitude of plunging motion (cm)
\bar{h}	Non-dimensional plunging amplitude, $\bar{h} = 2h_0/c$
U	Streamwise mean velocity (m/s)
α_{eq}	Equivalent angle of attack (deg)
α	Angle of attack (deg)

α_0	Initial angle of attack (deg)
α_{ds}	Dynamic stall angle of attack (deg)
α_{ms}	moment stall angle of attack (deg)
α_{ss}	static stall angle of attack (deg)
k	Reduced frequency $\pi fc/U_\infty$

Introduction

Turbine blade control can be of two types: passive control and active control. Passive control has been extensively used in the design of wind turbine blades; passively controlling the flow improves the performance of the turbine and mitigates the loads on the structure [1]. Active flap control systems of the wind turbine are used to mitigate excessive loads (extreme, fatigue, cyclic, etc.) caused by variations in the wind. However, the design of the active flap controllers is generally complicated and demands high

1. Assistant Professor

2. Professor (Corresponding Author)

costs of manufacturing and maintenance. In this study, a specific kind of passive flap control, called Gurney flap, is implemented to a plunging wind turbine blade section.

The Gurney flap is a simple device, consisting of a short strip, on the order of 1-5% of the airfoil chord in height, fitted perpendicularly to the pressure surface or the chord-line along the trailing edge of a wing. Race-car driver, Dan Gurney, used it on an inverted wing to increase the downward force in high-speed turnings. At first, an experimental study of the Gurney flap was conducted by Liebeck [2] on a Newman airfoil. According to Liebeck, Gurney flap with the height of 1.25% increased the lift substantially and slightly reduced the drag. Increasing the Gurney flap height beyond 2% of the chord continued to increase the lift, which caused substantial increase in the drag.

Storms and Jang [3] obtained the pressure distributions and wake profiles on an airfoil equipped with Gurney flaps. They observed that at high lift coefficients there was less drag, while more drag resulted from low to moderate lift coefficients.

Giguère et al. [4] studied the effect of Gurney flaps with the height of 0.5 to 5%, on LA203A and Göttingen797 airfoils. Based on their results, as well as a review of past studies, they found that the Gurney flap significantly increased the lift with a very small penalty in drag. They also found that the optimum Gurney flap height is scaled with the boundary layer thickness.

A comprehensive study on the effects of Gurney flaps for a wide range of configurations and test conditions was conducted by Myose et al. [5]. They used symmetric NACA 0011 and cambered GA (W)-2 airfoils during the single-element airfoil tests. Moreover, the GA (W)-2 airfoil was studied for slotted flap with 0, 10, 20 and 30 deflections. They indicated that the maximum lift enhancement was achieved for a 1% Gurney flap, and the maximum lift-to-drag ratio was increased by 21% for 1% c slotted flapped airfoil with 30deg deflection.

Jeffrey et al. [6] conducted laser Doppler anemometry (LDA) measurements downstream of a Gurney flap. The LDA data showed that the wake consisted of a Von Kármán vortex sheet of alternately shed vortices. The vortex shedding increased the suction at the trailing edge on the suction side of the airfoil. On the pressure side of the airfoil, the Gurney flap decelerated the flow and thus increased the pressure. The resulted pressure difference that occurred across the trailing edge increased the airfoil circulation.

Troolin et al. [7] investigated the velocity field details of the flapped airfoil by the time-resolved particle image velocimetry (PIV). Data showed that the two vortex shedding modes existed in a wake region behind the flap. The dominant mode resembled

the vortex street behind an asymmetric bluff body. The second mode related to an intermittent shedding of fluid within the cavity upstream of the flap, which became more coherent by increasing airfoil incidence.

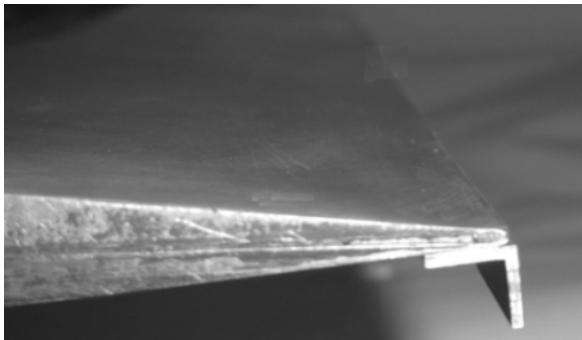
The extension of the Gurney flap concept to oscillating airfoil was reported by Geronatkos and Lee [8, 9]. They conducted a comprehensive study on the pitching airfoil with a trailing edge strip and an inverted strip. According to their results, the Gurney flap led to a significant increase in the unsteady lift force and nose-down pitching moment similar to the static flapped airfoil. In contrast to the Gurney flap, the inverted trailing edge strip alleviated negative damping while reducing the lift.

Tang and Dowell [10] computationally investigated the effects of small trailing-edge strips on the steady and unsteady flow for a NACA0012 airfoil using a Navier–Stokes code, INS2D. They studied the cases of a pitching airfoil with several fixed Gurney flap sizes and an oscillating Gurney flap with a fixed airfoil at higher angles of attack. For the Gurney flap oscillating cases, the computations showed that the separation position moved forward on the lower surface and backward on the upper surface of the airfoil for near the trailing edge regions.

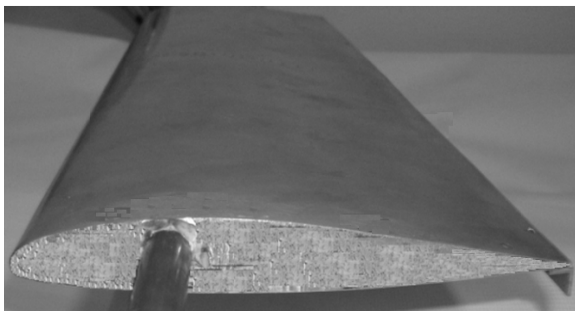
In the present study, the Gurney flaps with different heights ($h/c=0, 2.6, 3.3$ and 5%) are implemented on the wind turbine blade section which is plunged in the prior, within and post stall flow conditions. The major purpose of this survey is to investigate the Gurney flap effects on the aerodynamic loads hysteresis and dynamic stall flow phenomena of the plunging airfoil. It is of importance to note that the nature of the unsteady flow is very complicated and the flow phenomena are completely different from the static case. For an airfoil oscillated at angles higher than α_{ss} (static stall angle), the dynamic stall occurs. Dynamic stall phenomenon is one of the limiting factors, which affects the performance of helicopter rotor blades, wind turbines and high maneuvering aircrafts. It is characterized by the creation, convection and shedding of a leading edge vortex (LEV). As long as LEV is on the airfoil surface the produced lift is enhanced. However, when LEV is swept over the airfoil surface, the aft-moving center of pressure induces very large nose-down pitching moments [11]. Moreover, the addition of the Gurney flap on the plunging airfoil makes the flow field more complex. Hence, the investigations of the plunging wind turbine blade equipped with the Gurney flap are essential. It is noteworthy to mention that an improved knowledge of this field is necessary to design the active translational microtabs which are deployed along the wind turbine blade span because the design concept of these small tabs located near the trailing edge of a blade similar to the Gurney flaps.

Experimental Apparatus

The experiments were performed in a closed-circuit wind tunnel of $45 \times 45 \text{ cm}^2$ test section with the length of 120cm at Amirkabir University of Technology. The free-stream turbulence intensity in the test section was 0.1% at $U_\infty = 15 \text{ m/s}$ with the corresponding Reynolds number 1.5×10^5 . An Eppler361 airfoil, fabricated from solid aluminum with a chord length of 15cm and span of 45 cm, was mounted horizontally in the test-section. The gaps between the oscillating airfoil and the sidewall of the tunnel were set at less than 0.1cm in order to provide a two-dimensional uniform flow distribution. The airfoil was equipped with 51 pressure ports along the chord on the upper and lower surfaces. Three Gurney flap configurations with the heights of $h/c = 2.6, 3.3$ and 5% ($0.5\%c$ thickness) were installed perpendicular to the local curvature on the lower surface at the trailing edge of the model. Figure 1a and b show a view of the airfoil and Gurney flap, respectively.



a) Flapped airfoil

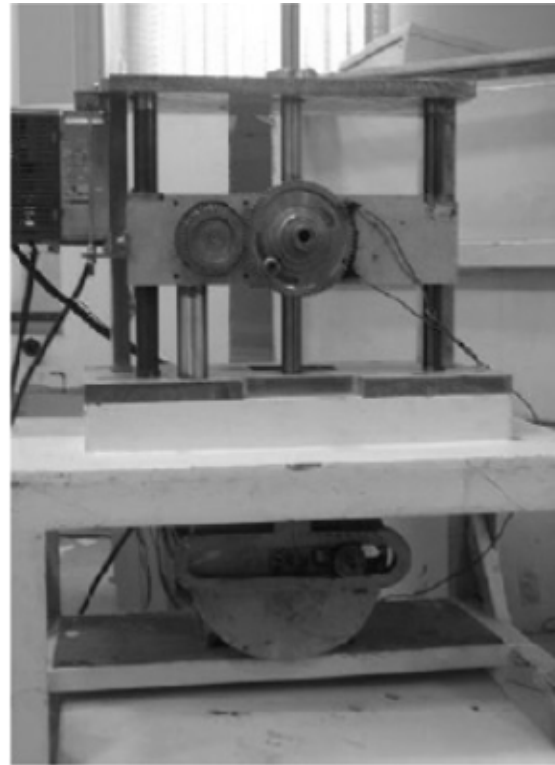


b) Gurney flap

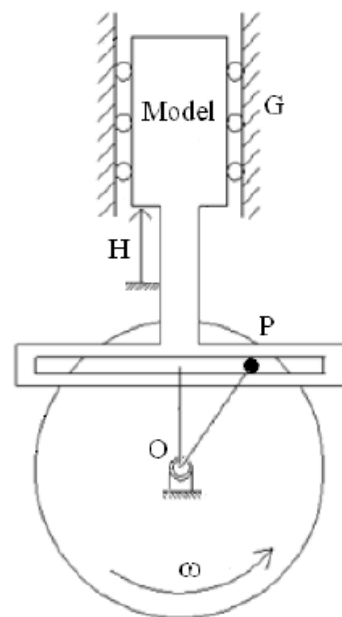
Figure 1. View of the airfoil

The Scotch-Yoke configuration was adopted to generate the plunging motion. This mechanism included a rotary motor with a cam follower and a yoke attached to the reciprocating element that converted circular motion of the motor into linear motion of the model. In this system, the position of the pin (point P) inside the yoke rotated about point O. The other end of the pin (point P), slide in the slot of the rod that reciprocated in the guide G. Different amplitudes of oscillations were provided by adjusting

the pin position. This mechanism could provide various frequencies (f), amplitudes (h_0) and initial angle of attack (α_0). The motor and gear combination developed a range of frequencies from 0.5 to 3Hz. Figures 2a and b illustrate the view and schematic of the oscillating mechanism, respectively.



a)



b)

Figure 2. View and schematic of the oscillating mechanism

The instantaneous displacement:

$H = h_0 \cos(\omega t)$ of the airfoil was recorded by using a potentiometer. The airfoil was oscillated with the reduced frequency of 0.073. For all of the tests the plunging amplitude of the oscillation was selected to be 6cm and the initial angles of attack were 0, 6, 10 and 12deg.

The surface pressure distributions were obtained using sensitive differential pressure transducers (HCXPM010D6V) with a quoted accuracy of 0.1% in the full-scale pressure range. The 51 pressure transducers were calibrated together with a definite pressure reference in order to find the relation between voltages and pressure variations. The trends of the variations for all of the sensors were linear with the slope of $\frac{\Delta p}{\Delta V} = 0.0019$. The pressure signals were ensemble-averaged over a large number of oscillations by the formula of $\bar{P} = \frac{1}{n} \sum_{i=1}^n p_i$, where n, \bar{P} and p are the number of the cycles, averaged pressure and instantaneous pressure, respectively. The aerodynamic load loops (C_l , C_d and C_m) are obtained by integrating the ensemble-averaged pressure signals. The pitching moment coefficients were calculated about the quarter chord for all the cases.

In order to eliminate the electrical noise from the raw data, output signals were digitally filtered using a low-pass filter. The cut-off frequency mainly depended on the noise level and the 25 Hz was chosen. Polyurethane tube with the length of 15 cm separated surface tap and the pressure transducers. The tubing had a simple time constant on all pressure signals on the order of millisecond which was inevitable in unsteady experimental tests.

The data process was performed on a PC with 12 bit A/D converter board. The output voltage of the potentiometer was synchronized with the pressure sensors outputs. The sampling frequency was 500Hz.

For the present experiments, several efforts had been made to minimize the related errors. The pressure sensors had been calibrated by the wind tunnel before and after each experiment in order to minimize the errors of variation in the sensor temperature. Accounting for statistical uncertainty [12], the maximum overall uncertainty of $\pm 1.2\%$ was expected for the pressure coefficients. All of the cited uncertainties were verified by repeatability. As an example, in figure 3 the error bar analysis is depicted on the unprocessed voltage signal of the port located at 1% from the leading edge.

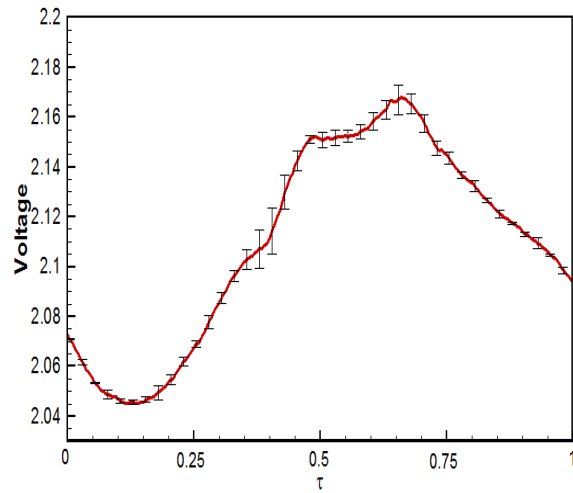


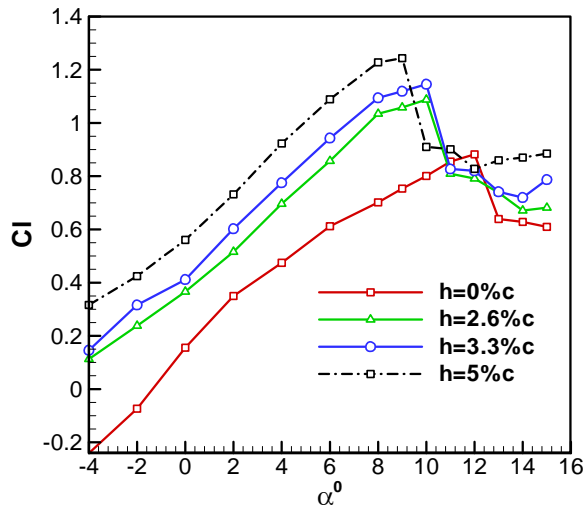
Figure 3. Error bar analysis of the port at 1% from the leading edge

Results and discussions

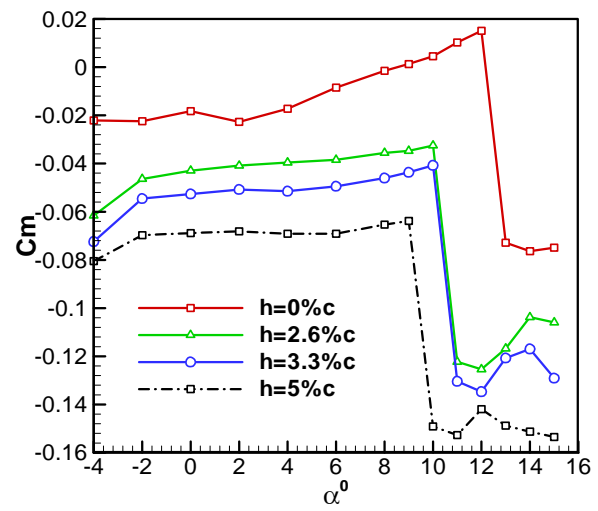
A series of experimental tests were conducted to assess the influence of Gurney flap upon the plunging airfoil loading. First, the aerodynamic loads of the static Eppler 361 airfoil equipped with Gurney flap ($h/c=0, 2.6, 3.3$ and 5%) were studied and they served as a reference for the flapped plunging airfoil. Secondly, the unsteady aerodynamic load characteristics of the plunging airfoil for the same flap heights at different regions according to McCroskey nomenclature [13] (prior to stall, stall onset, light stall and deep stall) were investigated.

Static Airfoil

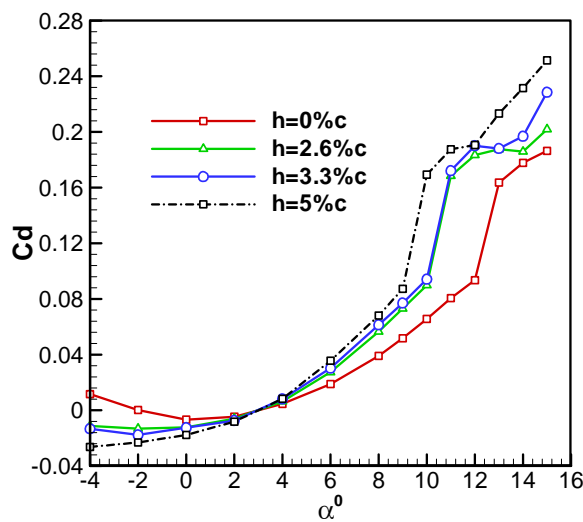
Figure 4 compares the aerodynamic coefficients and drag polar of the static flapped and unflapped airfoil. According to figure 4a, for the static unflapped airfoil a maximum lift coefficient $C_{l,max}$ of 0.88 with a linear lift-curve slope C_{l_α} ($=dC_l/d\alpha$ of 0.07) was obtained at a static-stall angle $\alpha_{ss} = 12$ deg. The pitching moment experiences a sharp fall from positive to negative values with a peak negative pitching-moment coefficient $C_{m,peak}$ of -0.073 (figure 4b). In figure 4c, a sharp rise of the drag coefficient C_d is also observed at α_{ss} . The drag polar presented in Figure 4d also indicates that the unflapped airfoil displayed a classical drag bucket. The maximum lift coefficient is observed at point C in the figure and the low drag is achieved from points A to B. It is worth noting that because of the sudden breaks in the lift and moment curve at α_{ss} the stalling mechanism is a sharp leading-edge stall type that is precipitated by the leading edge bubble bursting.



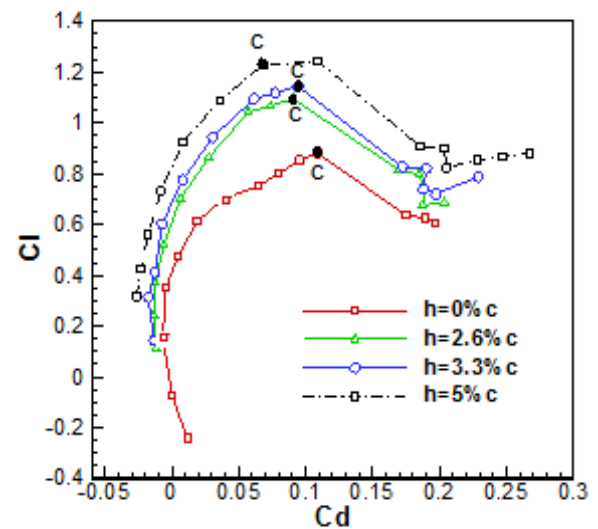
a) Lift force coefficient versus α



b) Pitching moment coefficient versus α



c) Drag force coefficient versus α



d) Lift force versus drag force coefficient

Figure 4. Gurney flap effects on static airfoil loads

According to figure 4, adding the Gurney flap the C_l axis shifts upwards for the complete ranges of incidences, including the after stall angle. It can be seen that the increase in lift is proportional to the size of the Gurney flap. Furthermore, the Gurney flap causes the zero lift angle of attack (α_0) and pitching moment to be more negative because of the positive camber effect of the flap (figure 4a,b). The α_{ss} is decreased further as a larger Gurney flap is utilized. The significant increase in the lift coefficient of Gurney flapped airfoils comes at the price of increased drag as shown in figure 4c. This is in agreement with the experimental results of the researchers [2-6] who conducted the tests of the different flap heights.

Comparisons between the drag polar diagram of the flapped and unflapped airfoil (figure 4d) indicate that the drag coefficient value of corresponding $C_{l,max}$ (point C) decreases for the flapped cases which is a positive effect in the airfoil performance. The variations of the critical static aerodynamic performance are summarized in table 1 for flapped and unflapped airfoils. From table 1, it is found that the Gurney flap promotes the stall phenomenon because at high initial angle the flap promotes a localized suction pressure peak in the leading-edge region and pushes the boundary layer closer to separation. It is notable that the stalling mechanisms are found to be similar to that of an unflapped airfoil.

Table 1. Comparison of the critical static aerodynamic performance

Flap heights (h/c)	α_{ss} , deg	Cl_{max}	Cl_{α}	α_0 , deg	Cm_{peak}	α_{ms} , deg	$L/D_{\alpha_{ss}}$
0%	12	0.88	0.07	-1.30	-0.073	12	9.36
2.6%	10	1.09	0.077	-5.08	-0.125	10	11.6
3.3%	10	1.14	0.078	-5.91	-0.133	10	12.12
5%	9	1.24	0.079	-7.53	-0.152	9	14.9

Dynamic Airfoil

The ensemble-averaged dynamic-load loops of an Eppler 361airfoil plunged with the amplitude of $H=6\text{cm}$ at $k=0.072$, are presented in figures 6-9 for both flapped and unflapped airfoils. The initial angles of attacks were 0, 6, 10 and 12deg. The angles were selected in a way that they could indicate the aerodynamic characteristics of the prior, within and beyond static stall of the airfoil. The data of the static airfoil for cases of $h/c=0\%$ and 5% are appended to the figures as a reference. The aerodynamic coefficients are presented in relation to the equivalent angle of attack (α_{eq}) which is described in the following.

The plunging displacement is transformed to the equivalent angle of attack by using the potential flow transformation formula: $\bar{\alpha}_{eq} = \tan^{-1}(\dot{H}/U_{\infty})$, which can be considered as $\bar{\alpha}_{eq} = \dot{H}/U_{\infty}$ for the small induced angles. \dot{H} is the uniform velocity perturbation normal to the chord and $\bar{\alpha}_{eq}$ is the induced angle of attack that airfoil actually sees during the oscillation cycle. Substituting \dot{H} in terms of reduced frequency gives $\bar{\alpha}_{eq} = k\bar{h} \sin(\omega t)$ where $\bar{\alpha}_{eq}$ is in radian and \bar{h} has been non-dimensionalised with the airfoil semi-chord $\bar{h} = 2h_0/c$. Figure 5 illustrates the cosinusoidal displacements of the plunging airfoil and the equivalent angle of attack (α_{eq}) variations at $\alpha_0=0\text{deg}$ in one cycle of oscillation. As it is shown in figure 5, plunging displacement of the airfoil has a ninety-degree phase lead with an equivalent angle of attack. It can be seen that α_{eq} is the maximum or minimum whenever $H=0$ during down-stroke and upstroke motions respectively.

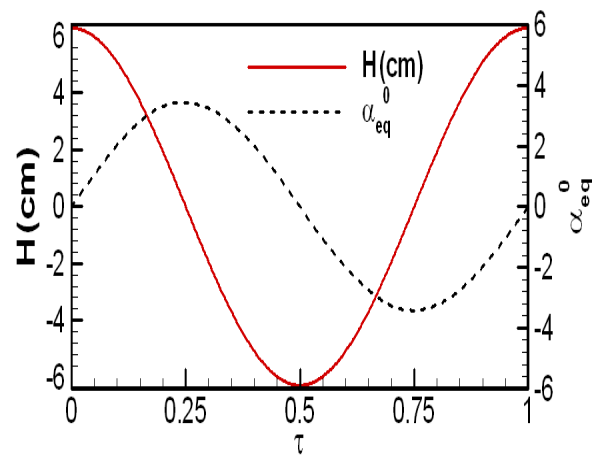


Figure 5. Time history of plunging motion with corresponding equivalent angle at $\alpha_0=0\text{deg}$

Figure 6 compares the aerodynamic load loops of flapped and unflapped plunging airfoils at $\alpha_0=0\text{deg}$ (prior the static stall). In this case, the equivalent angle of attack which shows the instantaneous position of the airfoil varies within the ranges of $-3.3 \text{ deg} < \alpha_{eq} < +3.3 \text{ deg}$. The directions of Cl and Cm hysteresis loops are counter clockwise, whereas the hysteresis loop for Cd is clockwise. Elliptical variations of the aerodynamic load loops indicate the attached flow conditions. The hysteresis of the load curves is originated from the airfoil bound vortices sheddings which induce lag effects in lift and moment distribution during one oscillation cycle. Consequently, the lift and moment are lower than the steady value when α_{eq} increases and higher than the steady value when α_{eq} decreases.

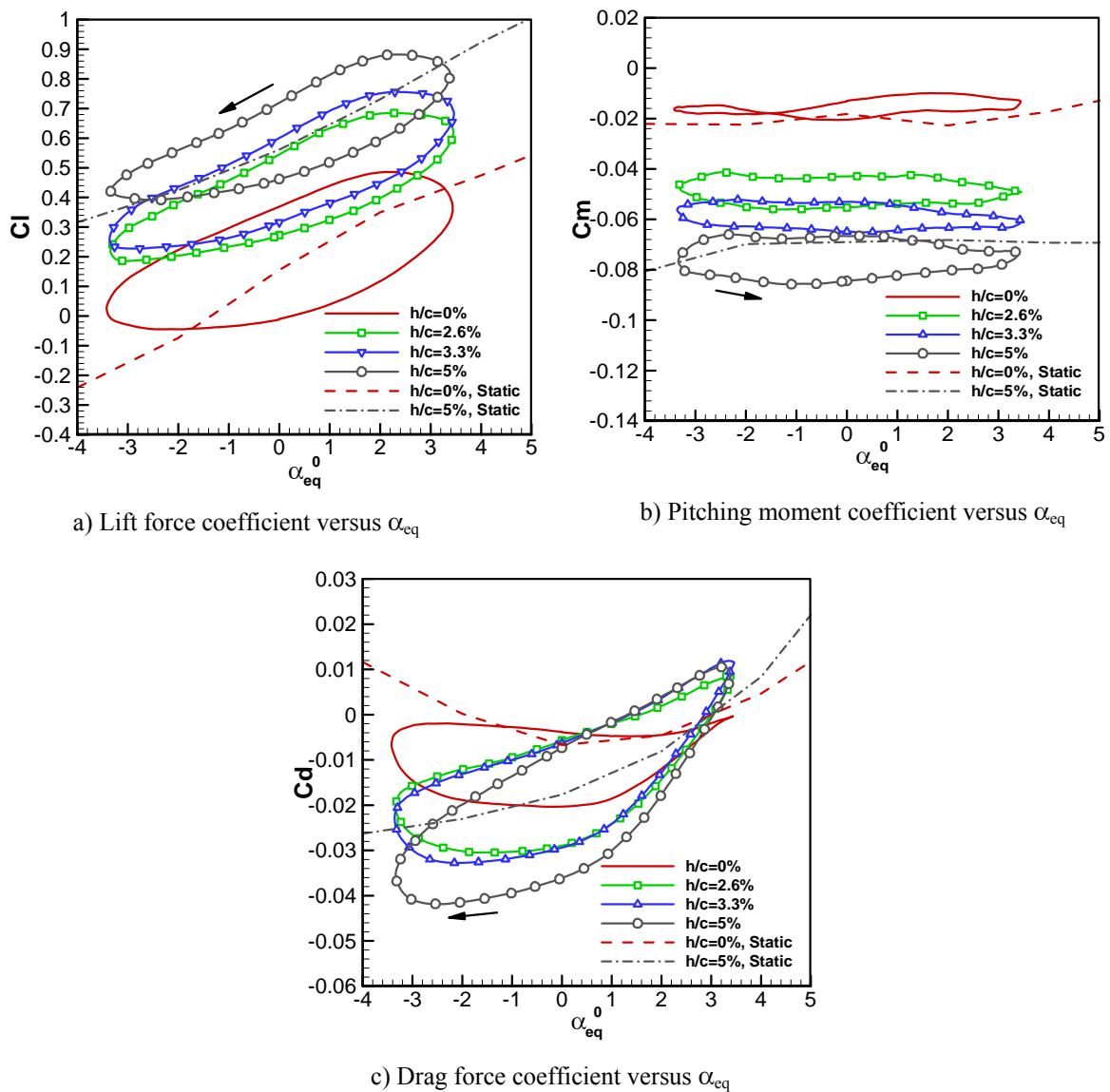


Figure 6. Gurney flap Effects on the dynamic load-loops for $\alpha_0=0\text{deg}$ at $k=0.072$

By adding the Gurney flap, the elliptical loops of the lift coefficient keep the same direction and shift vertically upwards. Furthermore, no significant changes either in the width or in the major axis slope of the lift loops are observed for the flapped airfoils (figure 6a), meanwhile, the maximum lift coefficient Cl_{max} is increased. For example, the maximum lift coefficient Cl_{max} of the dynamic cases for the flap heights of $h/c=0, 2.6, 3.3$ and 5% are $0.48, 0.68, 0.75$ and 0.88 at $\alpha_{eq}=2.3\text{deg}$. It is worth noting that the maximum lift coefficient Cl_{max} of all of the dynamic cases is not seen at maximum equivalent angle of $\alpha_{eq}=3.3\text{deg}$. As a result of the unsteady motion, the flapped and unflapped airfoils do not follow the flow at the same time; thus the maximum lift coefficient angle is not corresponded with the maximum equivalent angle of attack.

The trends of the pitching moment coefficients are completely different, so that the loops are shifted downwards and provide an undesirable increase in the nose-down pitching moment. Moreover, loop widths are increased remarkably by increasing the flap height (figure 6b). The notable pitching moment hysteresis of the greater flap height is attributed to the increase in both suction on the upper and positive pressures on the lower surfaces. In figure 6c, the main axis slope of the drag loop is increased for the flapped case in comparison with the unflapped one, where this effect is more pronounced with increasing the flap height.

In figure 7 the aerodynamic load loops of the flapped ($h/c=0, 2.6, 3.3$ and 5%) and unflapped airfoil are compared at $\alpha_0=6\text{deg}$. The variations range of the equivalent angle of attack is $2.7\text{deg} < \alpha_{eq} < 9.3\text{deg}$ in this case. As it is evident, the initial angle has been added

to the equivalent angle of attack. These same trends could be found in the hysteresis load loops directions of figures 6 and 7 for both flapped and unflapped airfoils. It indicates that the flow over the airfoil at ($\alpha_0=0$ and 6deg) does not experience very different boundary layer phenomena. Nevertheless, in contrast to figure 6b, the pitching moment hysteresis loop width is found to decrease significantly with increasing the flap height from $h/c=0\%$ to 5% . It is of interest to note that even

though the shapes of pressure drag hysteresis loops in figure 7c do not change with increasing the flap height, there is an increase in the main axis slope of the pressure drag loop. Furthermore, the minimum pressure drag of flapped and unflapped cases do not render any noticeable changes at $\alpha_{eq}=-3.3\text{deg}$, while the maximum pressure drag is increased from the value of 0.058 for the unflapped airfoil to 0.11 for the flapped case of $h/c=5\%$.

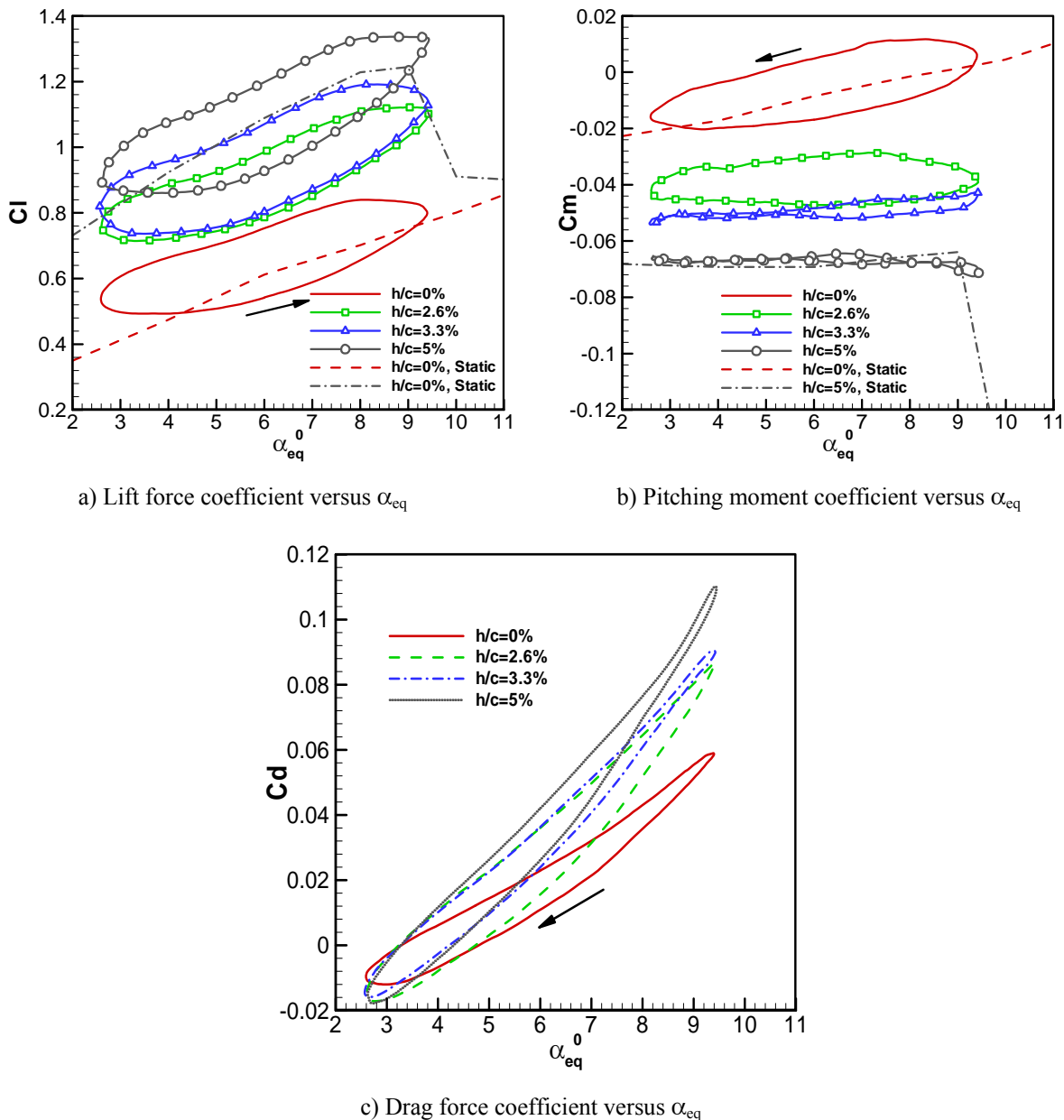


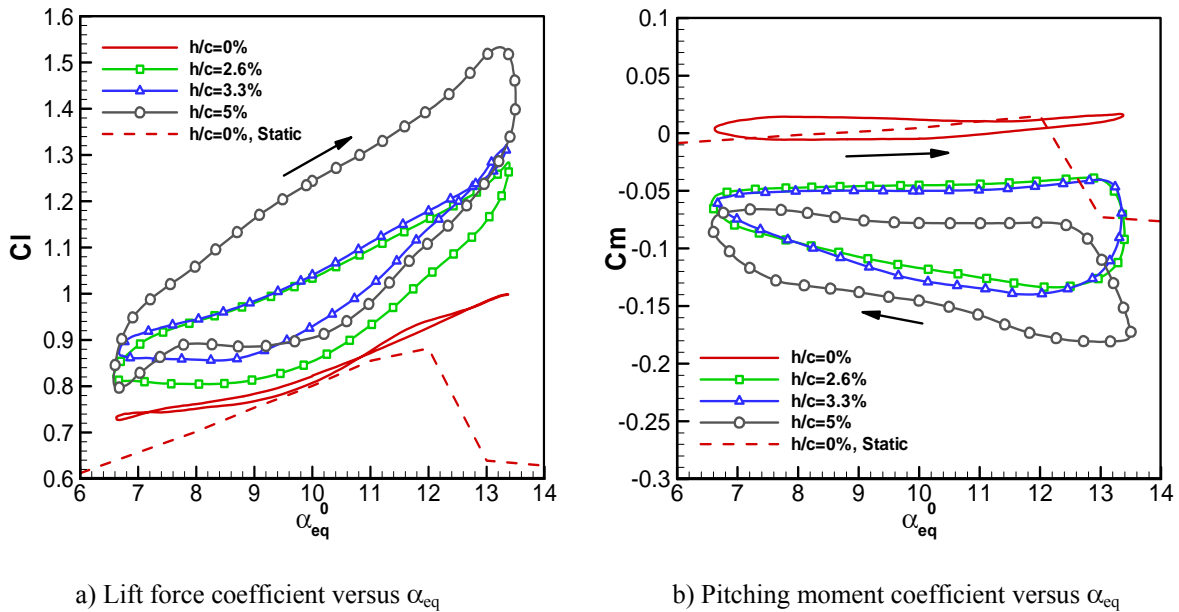
Figure 7. Gurney flap Effects on the dynamic load-loops for $\alpha_0=6\text{deg}$ at $k=0.072$

The dynamic hysteresis loops trends of flapped and unflapped plunging airfoil are investigated in figure 8 at initial angle of attack of $\alpha_0=10\text{deg}$. The equivalent angle of attack varies in the range

of $6.7\text{deg} < \alpha_{eq} < 13.3\text{deg}$. As a result of the separated flow on the unflapped oscillating airfoil surface in most of the oscillation cycle, the lift and pitching moment hysteresis loop keep the counterclockwise

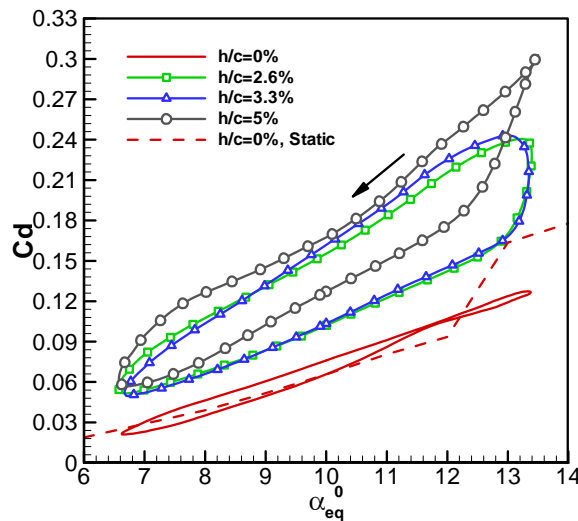
direction, exhibiting less width and deviating from a pure elliptical shape. These flow characteristics

describe stall onset regimes as discussed by McCroskey [13].



a) Lift force coefficient versus α_{eq}

b) Pitching moment coefficient versus α_{eq}



c) Drag force coefficient versus α_{eq}

Figure 8. Gurney flap Effects on the dynamic load-loops for $\alpha_0=10\text{deg}$ at $k=0.072$

The addition of Gurney flap results in a profound increase in the hysteresis of C_l and C_m loops (figure 8a, b). Furthermore the rotating direction of lift and pitching moment hysteresis loop changes into clockwise, which indicates that the boundary layer undergoes different flow phenomena, as compared to figures 6 and 7. The results indicate that like the static airfoil, adding the Gurney flap promotes the occurrence of dynamic stall phenomena, while increases the lift coefficient significantly. The dynamic

stall events occur for an airfoil oscillating beyond the (α_{ss}). In this process, the rear-to-front spread of the trailing edge flow reversal happens, then the boundary-layer is suddenly broken down and the energetic clockwise LEV (leading edge vortex) is formed. The LEV grows and convects rapidly to downstream with further increase in the airfoil incidence [11]. Consequently, a massive separation occurs on the airfoil. The presence of the promoted LEV is confirmed as the change in the direction of lift and

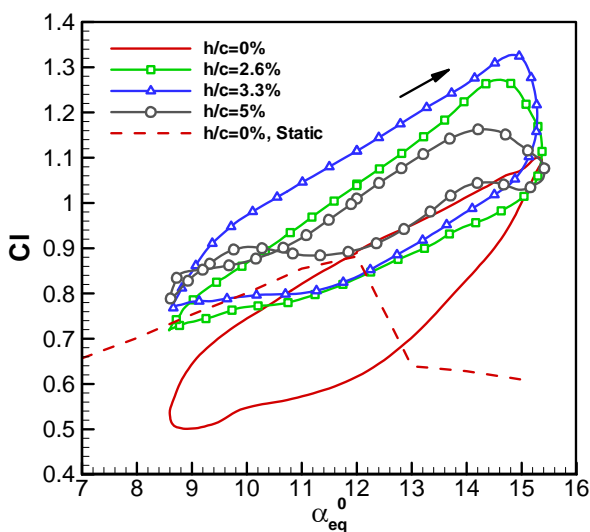
pitching moment hysteresis loop into clockwise occurs for the flapped airfoils. It is of importance to note that the flapped airfoils with the heights of 2.6 and 3.3% experience a light stall, while the boundary layer changes of flapped case ($h/c=5\%$) are so that they include a deep stall flow phenomena. More importantly, The LEV spillage of the flapped case ($h/c=5\%$) leads to a deep dynamic lift stall at $\alpha_{eq}=13.1\text{deg}$ with a maximum C_l of 1.53 (or a 39% increase in $C_{l,max}$) as compared to $C_{l,max}=1.1$ of the unflapped airfoil.

According to figure 8b, adding the Gurney flap, adversely increases both the undesirable effects of the negative pitching moment and the hysteresis loops width. The formation of the LEV, which corresponds with the sudden break in pitching moment coefficient [11] seen at $\alpha_{eq}=12.2\text{deg}$ for the $h/c=5\%$ flapped case, reaches to a peak value of $C_{m,peak}=-0.18$. This value is reported at $\alpha_{eq}=13\text{deg}$ for the cases of $h/c=2.6$ and 3.3% which approves the fact that with the addition of the Gurney flap dynamic stall phenomena and LEV formation are promoted. The peak nose-down C_m of -0.13 and -0.14 are noticed for the $h/c=2.6\%$ and 3.3% flapped airfoils, respectively. It is of importance to note that the LEV strength is relatively low for the $h/c=2.6$ and 3.3% flapped cases due to the inadequate time for full development of the LEV during the increase in the equivalent angle of attack (figures 8a, b). Thus, convection of the vortex along the chord occurred in decreasing equivalent angle of attack stroke. It should be noted that no dynamic moment and lift stall is observed for the unflapped airfoil.

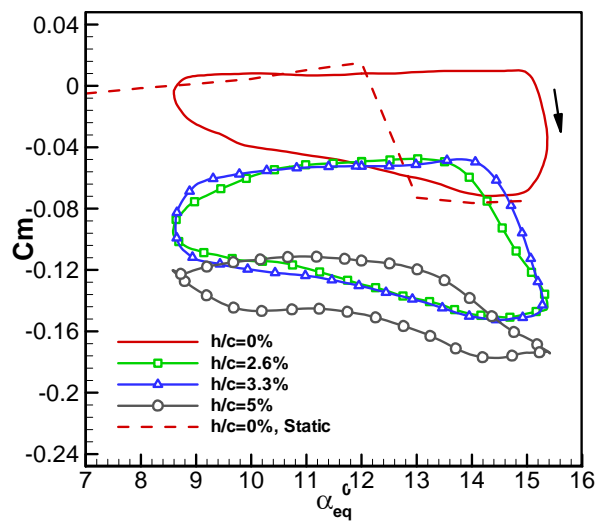
The influence of the Gurney flap on the pressure drag coefficient hysteresis loops is seen in figure 8c. According to the light stall flow characteristics [13], no significant hysteresis in the drag coefficient of unflapped airfoil is observed while the drag hysteresis

loop widths of the flapped airfoils increase remarkably and the sign changes to clockwise. The described changes in the drag coefficient trends are also attributed to the promotion of the dynamic stall flow phenomena. The discussed results reveal that the addition of Gurney flap not only intensifies the shear layers separating both upper and lower surfaces of the airfoil but also induces a rapid formation of the LEV during the cycle [14 and 15]. Consequently, in spite of the profound increase in the dynamic lift coefficient levels, a significant drag rise is induced. For example, the peak value of $C_{d,max}=0.3$ is found for the flapped $h/c=5\%$ case shows a 2.4 times increase as compared to the unflapped airfoil. However, less severe drag rises are produced for the $h/c=2.6$ and 3.3% cases.

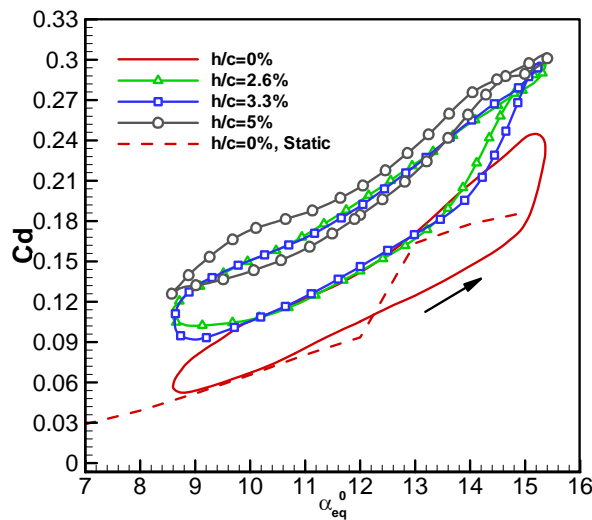
The load hysteresis profiles of plunging flapped and unflapped airfoils are shown in figure 9 for the initial angle of attack of 12deg . In this case the equivalent angle of attack variations range is $8.7\text{deg} < \alpha_{eq} < 15.3\text{deg}$. The hysteresis patterns of the lift coefficient loops in figure 9a indicate that the unflapped oscillating airfoil experiences dynamic stall phenomena while the flapped airfoils with the height of $h/c=2.6$ and 3.3% encounter the deeper stall flow condition compared to an unflapped one. For the flapped $h/c=5\%$ airfoil, the levels of lift coefficients reduce substantially in most parts of the oscillation cycles so that no sharp gradient is seen at a high equivalent angle of attack. Moreover, the lift, pitching moment and pressure drag coefficients loops width are decreased as compared to the flapped $h/c=2.6$ and 3.3% cases; these changes exhibit after the deep dynamic stall flow conditions. Note that the lift and pitching moment coefficient hysteresis loops directions are clockwise for all cases (figures 9a and b).



a) Lift force coefficient versus α_{eq}



b) Pitching moment coefficient versus α_{eq}



c) Drag force coefficient versus α_{eq}

Figure 9. Gurney flap Effects on the dynamic load-loops for $\alpha_0=12deg$

From figure 9a, the maximum lift coefficients of $Cl_{max} = 1.26, 1.33$ and 1.16 are observed for the cases $h/c=2.6, 3.3$ and 5% which indicate $14.5, 21$ and 5.4% increase in comparison with the unflapped airfoil ($h/c=0\%$). Evidently, the least increase in the amount of lift coefficient is related to the flapped $h/c=5\%$ airfoil because of the after deep stall flow condition and the maximum increment is for the flapped $h/c=3.3\%$ airfoil. In the meantime, after the dynamic lift stall at $\alpha_{eq}=14.8deg$ (for the flapped $h/c=2.6$ and 3.3%) the lift coefficient decreases with a sharp gradient and the first indications of the flow reattachment are observed at $\alpha_{eq}=9.6deg$ in decreasing the equivalent angle of attack. Note that the unflapped oscillating airfoil experiences an alleviated lift decrease in the lift stall angle ($\alpha_{eq}=15.3deg$).

According to figure 9b, the formation of the LEV is observed at $\alpha_{eq}=15$ and $13.9deg$ (moment stall angle) for the unflapped and flapped ($h/c=2.6$ and 3.3%) airfoils, respectively which indicates the occurrence of the most LEV displacements before the beginning of the decrease in the equivalent angle of attack. The increased Cl_{max} of flapped ($h/c=2.6$ and 3.3%) airfoils costs of more negative pitching moment of $Cm_{peak} = -0.15$.

The variations of the aerodynamic critical values of flapped and unflapped plunging airfoil are summarized in table 2. It can be clearly seen that the critical values related to the loads increase with the flap height and those related to incidences are promoted. The greater flap height leads to an increase in the degree of asymmetry or hysteresis in the dynamic load loops in its deep stall flow condition as compared to an unflapped airfoil.

Table 2. Comparison of the critical dynamic aerodynamic performance

Flap heights (h/c)	Cl_{max}	Cd_{max}	Cm_{peak}	$\alpha_{ds, deg}$	$\alpha_{ms, deg}$
0%	1.1	0.24	-0.07	15.3	15
2.6%	1.26	0.27	-0.15	14.8	13.9
3.3%	1.33	0.27	-0.15	14.8	13.9
5%	1.53	0.3	-0.18	13.1	12.2

Conclusions

The dynamic load loops of a plunging Eppler 361 airfoil were studied at the regions prior to stall, stall onset, light stall and deep stall for the flapped and unflapped airfoils to obtain the following conclusions.

Static Gurney flapped airfoil

The airfoil with the Gurney flap had higher lift coefficient, more negative zero lift angle of attack, and nose down pitching moment with a penalty in drag coefficient. The lower flap height rendered a lower penalty in aerodynamic coefficients. Moreover, inclusion of the Gurney flap promoted the occurrence of the stall phenomena. Hence, according to the results the airfoil with the height of 3.3 made a better aerodynamic efficiency as compared to the other cases.

Plunging Gurney flapped airfoil

In the phase prior to stall flow conditions which is similar to the static flapped airfoil, with the addition of the Gurney flap the Cl_{max} increased and the lift hysteresis loops shifted upwards due to the positive

camber effects. The negative effect of the Gurney flap on the load loops was the downwards displacements of the flapped pitching moment coefficients. No significant penalty in the drag coefficient was observed in this flow conditions.

The investigations of flapped and unflapped hysteresis load loops at $\alpha_0=10\text{deg}$ showed that the boundary layer underwent different flow phenomena for the flapped airfoil in comparison with the unflapped one, because the width of flapped airfoil load hysteresis loops increased significantly and the loops directions were opposite to the unflapped case. The addition of the Gurney flap, like static cases, promoted dynamic stall phenomena in a way that the flapped airfoil $h/c=5\%$ experienced a deep dynamic stall and other flapped cases ($h/c=2.6$ and 3.3%) encountered light stall flow conditions.

The addition of the Gurney flap promoted the formation, convection and spillage of the LEV and the flapped airfoils had a deep dynamic stall. Thus, oscillations of the airfoils at the initial angle of attack of 10deg rendered an improved aerodynamic efficiency regarding the penalty created.

References

1. Johnson S.J., van Dam C.P. "Case" and Berg D.E., , "Active load control techniques for wind turbines," SANDIA Report, 2008, SAND2008-4809.
2. Liebeck, R.H., 1978, "Design of subsonic airfoils for high lift," *Journal of Aircraft*, Vol. 15, pp. 547–551.
3. Storms, B.L. and Jang, C.S., "Lift enhancement of an airfoil using a Gurney flap and vortex generators", *Journal of Aircraft*, Vol. 31, 1994, pp. 542–7.
4. Giguère P., Dumas G., Lemay J., , "Gurney flap scaling for optimum lift-to-drag ratio," *AIAA Journal*, Vol. 35, 1997, pp.1888–1890.
5. Myose, R., Papadakis, M., and Heron, I., "Gurney flap experiments on airfoils, wings, and reflection plane model," *Journal of Aircraft*, Vol. 35, 1998, pp. 206-211.
6. Jeffrey, D., Zhang, X. and Hurst, D.W., "Aerodynamics of Gurney flaps on a single-element high-lift wing," *Journal of Aircraft*, Vol. 37, 2000, pp. 295–301.
7. Troolin D.R., Longmire E.K., Lai W.T., "Time resolved PIV analysis of flow over a NACA0015 airfoil with Gurney flap," *Experiments in Fluids*, Vol. 41, 2005, pp. 241–54.
8. Gerontakos P, Lee T., "Oscillating wing loadings with trailing edge strips," *Journal of Aircraft*, Vol. 43, 2005, pp. 428–435.
9. Gerontakos P., Lee T., "Particle image velocimetry investigation of flow over unsteady airfoil with trailing-edge strip," *Experiments in Fluids*, Vol. 44, 2008, pp. 539-555,.
10. Tang, D. and Dowell, E.H., "Aerodynamic flow control of an airfoil with small trailing-edge strips," *Journal of Aircraft*, Vol. 43, 2006, pp. 1854–1866.
11. Lee T., Gerontakos P., "Investigation of flow over an oscillating airfoil," *Journal of Fluid Mechanics*, Vol. 512, 2004, pp.313-341.
12. Thomas G.B. Roy D.M., John H.L., *Mechanical measurements*, Fifth Edition, Addison-Wesley.
13. McCroskey, W.J., "Unsteady airfoils," *Annual Reviews*, Vol. 4, 1995, 1982, pp. 285-311.
14. Ajalli F., Mani M., "Effects of adding strip flap on a plunging airfoil," *Aircraft Engineering and Aerospace Technology*, Vol. 86, 2014, pp.6-18.
15. Ajalli F., Mani M, Tadjfar M., "Plunging wake analysis of an airfoil equipped with a Gurney flap," *Experimental techniques journal*, Vol. 39, 2015, pp.48-60.